



Cellular Management of Zinc in Group B Streptococcus Supports Bacterial Resistance against Metal Intoxication and Promotes Disseminated Infection

 Matthew J. Sullivan,^{a,b}  Kelvin G. K. Goh,^{a,b}  Glen C. Ulett^{a,b}

^aSchool of Pharmacy and Medical Sciences, Griffith University, Gold Coast, Australia

^bMenzies Health Institute Queensland, Griffith University, Gold Coast, Australia

ABSTRACT Zinc is an essential trace element for normal bacterial physiology but, divergently, can intoxicate bacteria at high concentrations. Here, we define the molecular systems for Zn detoxification in *Streptococcus agalactiae*, also known as group B streptococcus, and examine the effects of resistance to Zn stress on virulence. We compared the growth of wild-type bacteria and mutants deleted for the Zn exporter, *czcD*, and the response regulator, *sczA*, using Zn-stress conditions *in vitro*. Macrophage antibiotic protection assays and a mouse model of disseminated infection were used to assess virulence. Global bacterial transcriptional responses to Zn stress were defined by RNA sequencing and quantitative reverse transcription-PCR. *czcD* and *sczA* enabled *S. agalactiae* to survive Zn stress, with the putative CzcD efflux system activated by SczA. Additional genes activated in response to Zn stress encompassed divalent cation transporters that contribute to regulation of Mn and Fe homeostasis. *In vivo*, the *czcD-sczA* Zn management axis supported virulence in the blood, heart, liver, and bladder. Additionally, several genes not previously linked to Zn stress in any bacterium, including, most notably, *arcA* for arginine deamination, also mediated resistance to Zn stress, representing a novel molecular mechanism of bacterial resistance to metal intoxication. Taken together, these findings show that *S. agalactiae* responds to Zn stress by *sczA* regulation of *czcD*, with additional novel mechanisms of resistance supported by *arcA*, encoding arginine deaminase. Cellular management of Zn stress in *S. agalactiae* supports virulence by facilitating bacterial survival in the host during systemic infection.

IMPORTANCE *Streptococcus agalactiae*, also known as group B streptococcus, is an opportunistic pathogen that causes various diseases in humans and animals. This bacterium has genetic systems that enable zinc detoxification in environments of metal stress, but these systems remain largely undefined. Using a combination of genomic, genetic, and cellular assays, we show that this pathogen controls Zn export through CzcD to manage Zn stress and utilizes a system of arginine deamination never previously linked to metal stress responses in bacteria to survive metal intoxication. We show that these systems are crucial for survival of *S. agalactiae* *in vitro* during Zn stress and also enhance virulence during systemic infection in mice. These discoveries establish new molecular mechanisms of resistance to metal intoxication in bacteria; we suggest these mechanisms operate in other bacteria as a way to sustain microbial survival under conditions of metal stress, including in host environments.

KEYWORDS *Streptococcus agalactiae*, bacterial pathogenesis, *czcD*, metal ions, metallobiology, zinc efflux

Citation Sullivan MJ, Goh KGK, Ulett GC. 2021. Cellular management of zinc in group B streptococcus supports bacterial resistance against metal intoxication and promotes disseminated infection. *mSphere* 6:e00105-21. <https://doi.org/10.1128/mSphere.00105-21>.

Editor Michael David Leslie Johnson, University of Arizona

Copyright © 2021 Sullivan et al. This is an open-access article distributed under the terms of the [Creative Commons Attribution 4.0 International license](https://creativecommons.org/licenses/by/4.0/).

Address correspondence to Glen C. Ulett, g.ulett@griffith.edu.au.

Received 3 February 2021

Accepted 23 April 2021

Published 19 May 2021

Inside living cells, zinc is an essential cofactor for metalloenzymes (1, 2) but is toxic at high concentrations, as can be encountered by bacteria inside phagocytes (3, 4). The

double-edged sword of essentiality and toxicity of Zn to bacteria is a burgeoning area of research due to the potential for antimicrobial applications (5–7). In the host, bacterial pathogens employ distinct mechanisms for internalizing essential Zn (8, 9), and, in turn, the host can restrict Zn availability as an antimicrobial strategy (10). Phagocytes can mobilize cellular Zn to expose internalized bacteria to metal concentrations that are antimicrobial (5, 11, 12). Host-driven Zn intoxication (defined as an excess of extracellular Zn) of bacterial pathogens can involve ablation of uptake of essential Mn (13), a compromised bacterial response to oxidative stress (14), or disrupted central carbon metabolism (15). Some bacteria can evade metal intoxication by mechanisms that involve metal efflux (16).

In streptococci, a specific genetic system manages Zn homeostasis by regulating metal import and export (13, 17). In pneumococcus and *Streptococcus pyogenes*, systems for Zn efflux pair a Zn-sensing transcriptional response regulator (*sczA*) with a Zn efflux transporter, encoded by *czcD* (17, 18). Here, we studied Zn management in *Streptococcus agalactiae*, also known as group B streptococcus, which is an important opportunistic pathogen that has undefined Zn detoxification systems and is associated with distinct disease etiologies compared to other streptococci. We establish a role for CzcD, as well as other novel factors, in mediating *S. agalactiae* resistance to Zn stress and virulence.

RESULTS

Excess Zn impedes *S. agalactiae* growth and disturbs cell physiology. Initial assays analyzed the growth of wild-type (WT) *S. agalactiae* strain 874391 (ST-17; serotype III) in a nutrient-rich Todd-Hewitt broth (THB) supplemented with moderate (0.5 mM), high (1.0 mM), and excess (1.5 mM) levels of Zn. High and excess Zn (≥ 1 mM) delayed exponential growth of the WT, with significant attenuation of the growth rate and final biomass yield (Fig. 1A). An isogenic $\Delta czcD$ mutant strain was significantly more susceptible to Zn at ≥ 1 mM (Fig. 1A). Full-length *czcD* supplied in *trans* to the mutant ($\Delta czcD + czcD$) restored growth to WT levels in Zn stress (Fig. 1A). Spot test assays of the bacteria on agar containing 0, 0.5, 1.0, and 1.5 mM Zn showed similar levels of susceptibility of the WT and $\Delta czcD$ strains on solid medium (Fig. 1B) compared to planktonic growth.

We next used a nutrient-limited medium to examine Zn stress in *S. agalactiae* in a modified chemically defined minimal medium (CDM), which likely more closely reflects a host environment (nutrient limited). CDM contained low basal levels of Zn ($0.11 \pm 0.03 \mu\text{M}$), as determined by inductively coupled plasma optical emission spectroscopy (ICP-OES). Growth assays of *S. agalactiae* in CDM with or without Zn supplementation revealed markedly enhanced Zn-induced toxicity compared to THB, with Zn being totally bacteriostatic to all strains at 0.5 mM (Fig. 1C). Similar to THB, growth of the $\Delta czcD$ mutant was significantly inhibited compared to that of the WT upon exposure to ≥ 0.1 mM in CDM (Fig. 1C).

Regulation of Zn efflux in *S. agalactiae*. The capacity of Zn stress to induce expression of *czcD* for Zn export was examined by analyzing mid-log-phase *S. agalactiae* grown with 0.25 to 1.5 mM supplemental Zn for 2.5 h prior to quantitative reverse transcription-PCR (qRT-PCR) quantification of *czcD*. *czcD* was significantly upregulated in response to Zn (3-fold to 18.9-fold) in a manner that was titratable with the Zn concentration (Fig. 2A) and consistent with a role for CzcD in responding to extracellular Zn. Interestingly, we identified a candidate gene, divergent from *czcD*, that encodes a putative Zn-responsive activator in the TetR family of transcription factors, termed streptococcal *czcD* activator, or *sczA* (19). Similar to $\Delta czcD$ *S. agalactiae*, a mutant deficient in *sczA* ($\Delta sczA$) was markedly more susceptible to Zn stress than the WT under both nutrient-rich and -limited conditions; the attenuation was restored by complementation *in trans* (Fig. 1).

To confirm the role of SczA as a Zn-responsive activator of *czcD* expression, we quantified *czcD* mRNA in $\Delta sczA$ *S. agalactiae* grown in 0.25 mM supplemental Zn (sub-inhibitory; to enable comparisons independent of metabolic state and alleviate

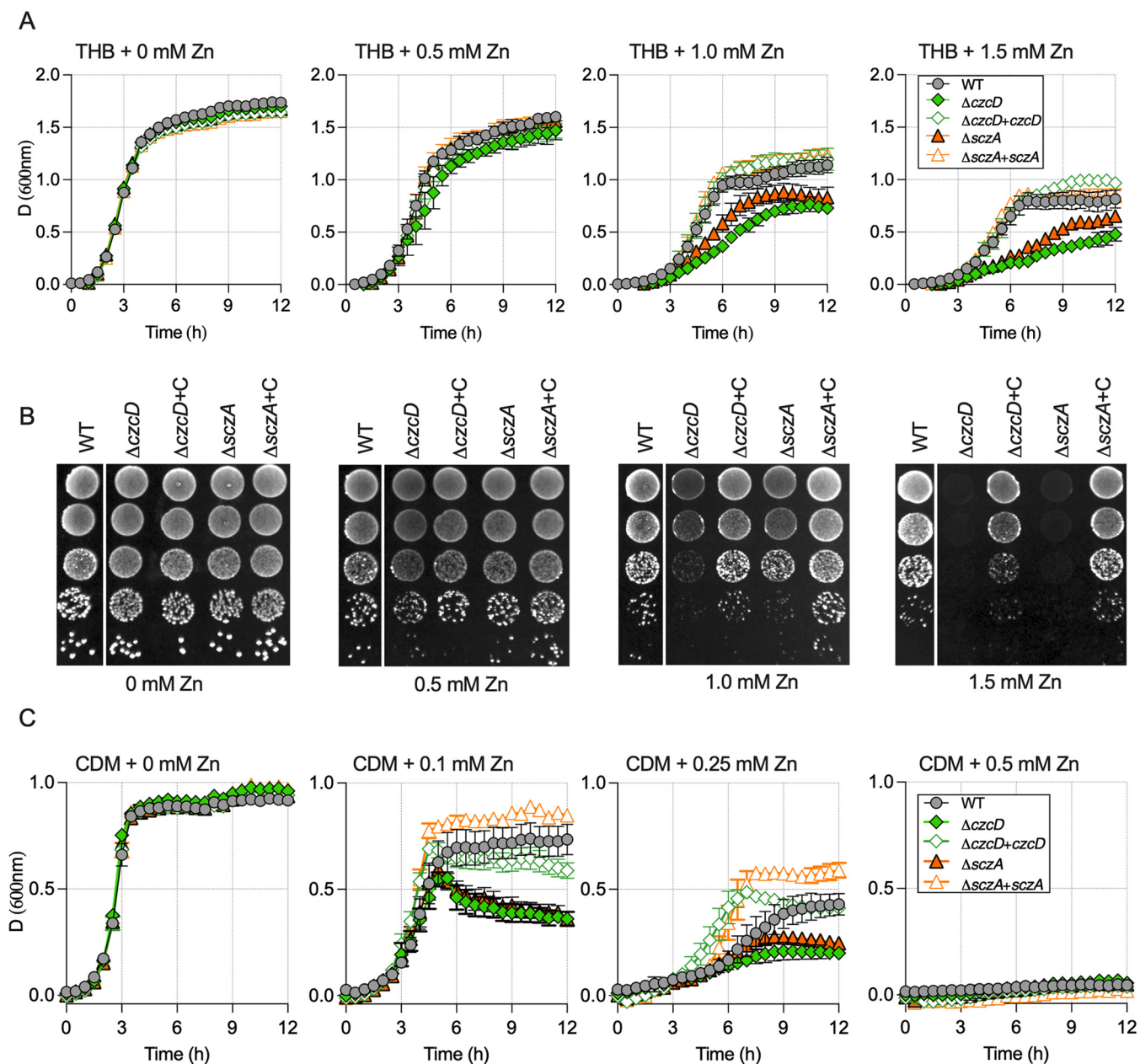


FIG 1 Comparison of the growth of WT *S. agalactiae*, $\Delta czcD$ and $\Delta sczA$ isogenic mutants, and complemented strains. (A) Growth curves of 874391 and mutant strains, as indicated, in Todd-Hewitt broth (THB) supplemented with 0, 0.5, 1.0, and 1.5 mM Zn. (B) Analysis of growth of *S. agalactiae* strains on solid TH medium with increasing Zn concentrations by serial dilution and droplets on agar. Composite images were spliced for labeling purposes. All five strains were imaged from the same agar plate for each Zn concentration. (C) Growth curves of 874391 and mutant strains, as indicated, in CDM supplemented with 0, 0.1, 0.25, and 0.5 mM Zn. Data shown are mean measurements of attenuation (D ; at 600 nm) from 3 to 4 independent experiments, and bars show standard errors of the means (SEM).

potential bias from any discordant Zn stress between WT and mutants with varied resistance phenotypes). Deletion of *sczA* significantly perturbed activation of *czcD* in response to Zn (Fig. 2B), consistent with previous reports of *SczA* functioning as a Zn-dependent activator of *czcD* in *S. pyogenes* and *S. pneumoniae* (17, 18).

Intracellular Zn content in *S. agalactiae* during Zn stress. We analyzed accumulation of Zn ions within the bacteria following Zn stress by using growth conditions equivalent to those for transcriptional experiments. WT, $\Delta czcD$, and $\Delta sczA$ *S. agalactiae* were grown in 0.25 mM supplemental Zn for 2.5 h prior to quantifying intracellular metal content by ICP-OES. In the WT strain, Zn stress caused accumulation of

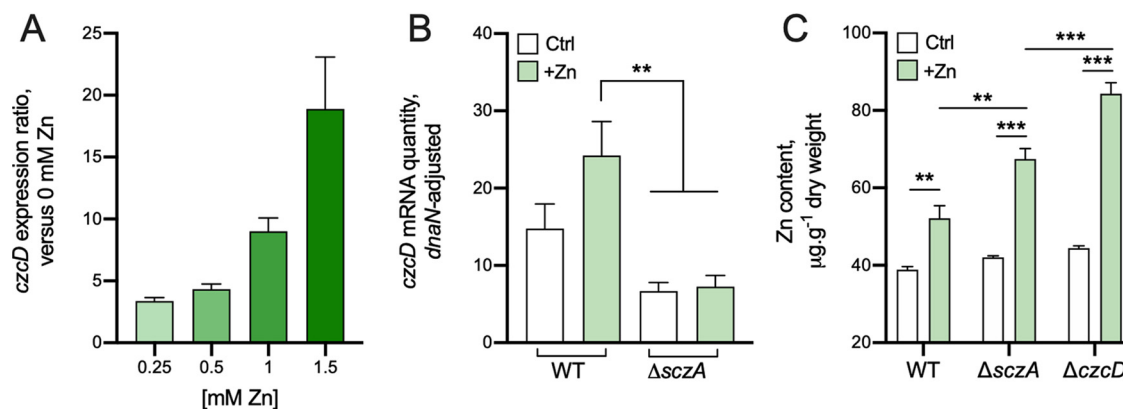


FIG 2 Expression analysis of *czcD* and intracellular Zn content in *S. agalactiae* strains. (A) Expression ratio of *czcD* quantified by qRT-PCR in THB medium containing 0.25, 0.5, 1.0, and 1.5 mM Zn compared to THB without Zn. (B) Relative *czcD* transcripts were quantified in WT and $\Delta sczA$ strains with and without Zn supplementation. (C) Intracellular accumulation of Zn was compared with and without Zn supplementation in WT, $\Delta sczA$, and $\Delta czcD$ strains. Ratios in panel A were calculated, as described previously (45), using C_T values, primer efficiencies, and housekeeping *dnaN*. In panels B and C, Ctrl, THB + 0 mM; +Zn, THB + 0.25 mM Zn. Bars show means and SEM from 3 to 4 independent experiments and compared by one-way analysis of variance (ANOVA) with Holm-Sidak multiple comparisons (**, $P < 0.01$; ***, $P < 0.001$).

intracellular Zn (52.1 versus 38.8 $\mu\text{g Zn/g}$ dry weight) compared to control cultures without supplemental Zn. In addition, intracellular Zn contents in $\Delta czcD$ and $\Delta sczA$ mutants grown under equivalent conditions were significantly enhanced (84.3 and 67.5 $\mu\text{g Zn/g}$ dry weight, respectively) compared to the WT in Zn stress or control incubations of the mutant strains without Zn (Fig. 2C). These findings are consistent with roles for CzcD and SczA as mediators of Zn efflux.

Resistance of intracellular *S. agalactiae* to Zn stress in macrophages. To determine if Zn efflux systems support survival of *S. agalactiae* in phagocytic cells, we used murine macrophages and human monocyte-derived macrophage-like cells in antibiotic protection assays at 1 h, 24 h, and 48 h of incubation. Viable intracellular *S. agalactiae* cells were reduced in number over the time course in human and murine cells, but no significant differences between WT, $\Delta czcD$, and $\Delta sczA$ strains were detected (Fig. 3A). To examine host-mediated Zn release inside phagocytic cells, we developed a system for expressing mCherry in *S. agalactiae*. We used this in concert with a Zn-binding fluorophore (FluoZin-3AM) to visualize intracellular *S. agalactiae* inside J774A.1 cells. Despite no effect of Zn efflux mutants on survival, we observed that *S. agalactiae* induced robust mobilization of Zn inside host cells at the 24-h time point compared to noninfected control incubations (Fig. 3B), as shown by enhanced detection and distribution of free Zn using FluoZin-3AM.

***S. agalactiae* Zn efflux systems contribute to virulence *in vivo*.** To examine the contribution of Zn efflux to *in vivo* colonization of *S. agalactiae*, we used a murine model of disseminated infection to monitor tissue and bloodstream burdens (20). Comparisons of the numbers of bacteria recovered from organs of mice that were challenged intravenously with 10^7 WT or mutant strains are shown in Fig. 4. We detected significantly fewer $\Delta czcD$ mutant cells in the liver ($P = 0.046$) and bladder ($P = 0.025$) than WT at 24 h postinoculation (Fig. 4A). No differences were observed between counts of the WT and $\Delta czcD$ mutant in the brain, blood, heart, lungs, kidneys, or spleen (see Fig. S3 in the supplemental material). In addition, significantly fewer $\Delta sczA$ mutant than WT cells were recovered from the blood ($P = 0.039$) and heart ($P = 0.032$) (Fig. 4B), indicating a modest but statistically significant role for cellular management of Zn via *czcD* and *sczA* in supporting disseminated infection *in vivo*.

***S. agalactiae* Zn stress transcriptome reveals new mediators of resistance.** The transcriptome of *S. agalactiae* in response to Zn stress was used to define the global response of this organism to externally applied Zn. RNA sequencing (RNA-seq) identified 567 genes that were differentially expressed during growth in 0.25 mM Zn (229

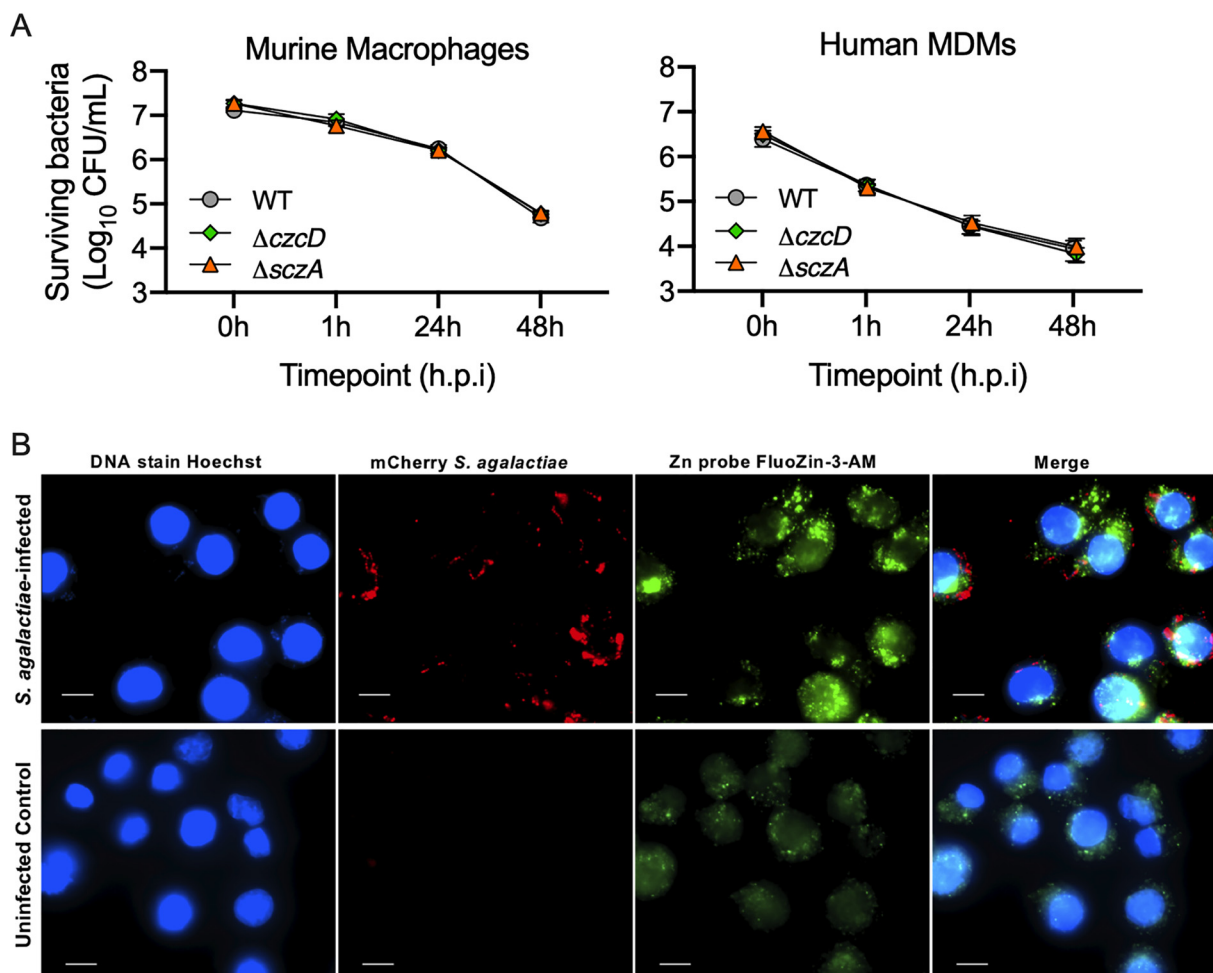


FIG 3 Interactions of *S. agalactiae* with macrophages and consequential mobilization of Zn. (A) Antibiotic protection assays with WT, $\Delta sczA$, and $\Delta czcD$ strains and mouse (J774A.1) or human (U937 monocyte-derived macrophage-like) macrophages, with surviving bacteria quantified at 0, 1, 24, and 48 h postinfection (h.p.i.). Data are means and SEM from 4 to 5 independent experiments. (B) Fluorescence imaging of the release of free Zn (detected using FluoZin-3 AM) by J774A.1 cells infected with WT *S. agalactiae* expressing mCherry from pGU2665 compared to noninfected J774A.1 cells at 24 h postinoculation. DNA was stained using Hoechst 33258. Scale bars, 10 μm .

up-, 238 downregulated; ± 2 -fold; adjusted P value [P -adj], < 0.05 ; $n = 4$ biological replicates) in WT *S. agalactiae* (Fig. 5A and Table S4). In addition to upregulation of *czcD*, we detected upregulation of several putative nickel and manganese transport loci (*nikABCD*, *mntH2*, and *mtsABC*, respectively) and downregulation of an iron efflux system (*fetAB*) and Zn-importing *adcA* (Fig. 5B). Interestingly, genes encoding transporters for nickel (*nikABCD*), zinc (*adcA*), and Mn (*mntH* and *mtsABC*) were recently implicated in *S. agalactiae* survival against host-derived calprotectin (21), which mediates Zn starvation, as opposed to Zn intoxication.

To provide functional insight into the observed changes in metal transporters, we analyzed cellular metal content of *S. agalactiae* during Zn stress for other second-row transition metals, including Mn, Fe, Ni, and Cu. We saw significant reductions in Mn levels, enhanced cellular Fe, and no difference in Cu levels, and Ni was below the detection limit (0.8 ppm) (Fig. 6A) for cultures of WT bacteria under Zn stress (0.25 mM) compared to nonsupplemented controls (THB medium only); we observed no difference in the levels of Mn, Fe, and Cu in comparing the WT to the $\Delta czcD$ or $\Delta sczA$ mutant (Fig. 6A). Given the reduction in Mn during conditions of Zn stress, we undertook experiments in which we supplied Mn in excess (0.5 mM) in addition to supplemental

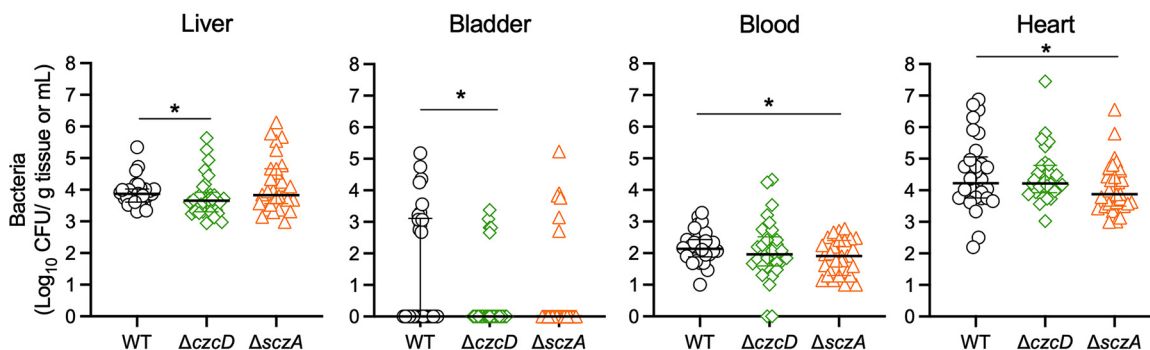


FIG 4 Virulence of WT (gray circles), $\Delta czcD$ (green diamonds), and $\Delta sczA$ *S. agalactiae* (orange triangles) strains in a mouse model of disseminated infection. C57BL/6 mice (6 to 8 weeks old) were intravenously injected with 10^7 bacteria; bacteremia and disseminated spread to the heart, liver, and bladder were monitored at 24 h postinfection. CFU were enumerated and counts were normalized using tissue mass, in grams. Lines and bars show median and interquartile ranges, and data are pooled from 3 independent experiments, each containing $n=10$ mice, with mutant strains compared using Mann-Whitney U tests to WT colonization data (*, $P < 0.05$; **, $P < 0.01$).

Zn and observed a complete rescue of the Zn sensitivity phenotypes of both the WT and $\Delta czcD$ strains (Fig. 6B).

In addition to metal transporters, we detected modulation of several metabolism-related gene clusters that have not previously been linked to Zn stress in bacteria, encompassing *de novo* nucleotide synthesis and import systems (*carAB*, *pyrB*, *pyrFEC*, *pur* genes, *uraA*, *nrdFIA*, and *guaC*) and riboflavin synthesis (*ribDEAH*) loci (Fig. 5 and Table S4). Interestingly, a putative arginine deaminase system (ADI), encoded by the *arcABCD* genes, was significantly upregulated (21- to 29-fold) under Zn intoxication (*arcA* highlighted in Fig. 5B). The *arcABC* genes encode arginine deaminase (ArcA), ornithine carbamoyltransferase (ArcB), and carbamate kinase (ArcC), with *arcD* encoding an ornithine/arginine antiporter. This system functions to produce ammonia and ATP from the conversion of arginine to ornithine, as characterized in *S. pneumoniae* (22), and is responsive to numerous stimuli (23).

We generated an isogenic $\Delta arcA$ mutant to examine a potential role for ADI in Zn stress resistance in *S. agalactiae*. Comparing the growth of the $\Delta arcA$ mutant to the WT under nutrient-limiting CDM plus 0.1 mM Zn (conditions in which $\Delta czcD$ and $\Delta sczA$ strains were perturbed) revealed significant attenuation of the $\Delta arcA$ strain for growth under Zn stress (Fig. 7A and Fig. S4). We used CDM, which normally contains 0.39 mM L-arginine, to confirm that *S. agalactiae arcA* has a role in arginine metabolism. We monitored growth of the WT compared to the $\Delta arcA$ mutant using CDM with or without supplementation with 10 mM L-arginine or L-ornithine (Fig. 7B). Final biomass yield was significantly elevated in WT cultures supplemented with L-arginine compared to the $\Delta arcA$ mutant, which showed no enhancement of growth with added L-arginine. Next, we reasoned that the products of arginine deamination confer an advantage to surviving Zn intoxication in *S. agalactiae*. To examine this, we analyzed growth in CDM supplemented with 0.25 mM Zn (severely inhibitory to WT) and supplied either L-arginine or L-ornithine, as described above. Strikingly, we saw that addition of L-ornithine rescued the Zn sensitivity phenotype of WT *S. agalactiae* during intoxication by 0.25 mM Zn, a phenomenon that was not observed in the $\Delta arcA$ strain (Fig. 7C). Addition of L-arginine was modestly inhibitory to the WT during intoxication by 0.25 mM Zn (Fig. 7C).

Finally, *S. agalactiae* modulated several genes encoding classical virulence and/or immunogenic factors in response to Zn intoxication, including the *cyl* gene cluster *cylXDG-acp-cylZABEFIJK* (encoding β -hemolysin/cytolysin) (2.5- to 4.3-fold down), *IrrG* (25-fold up, leucine-rich repeat protein), and *essABC* (11- to 22-fold down, type VII secretion system) (Table S4). We also note that $\sim 20\%$ of all transcripts (114/567) that were differentially regulated in response to Zn intoxication are predicted to encode

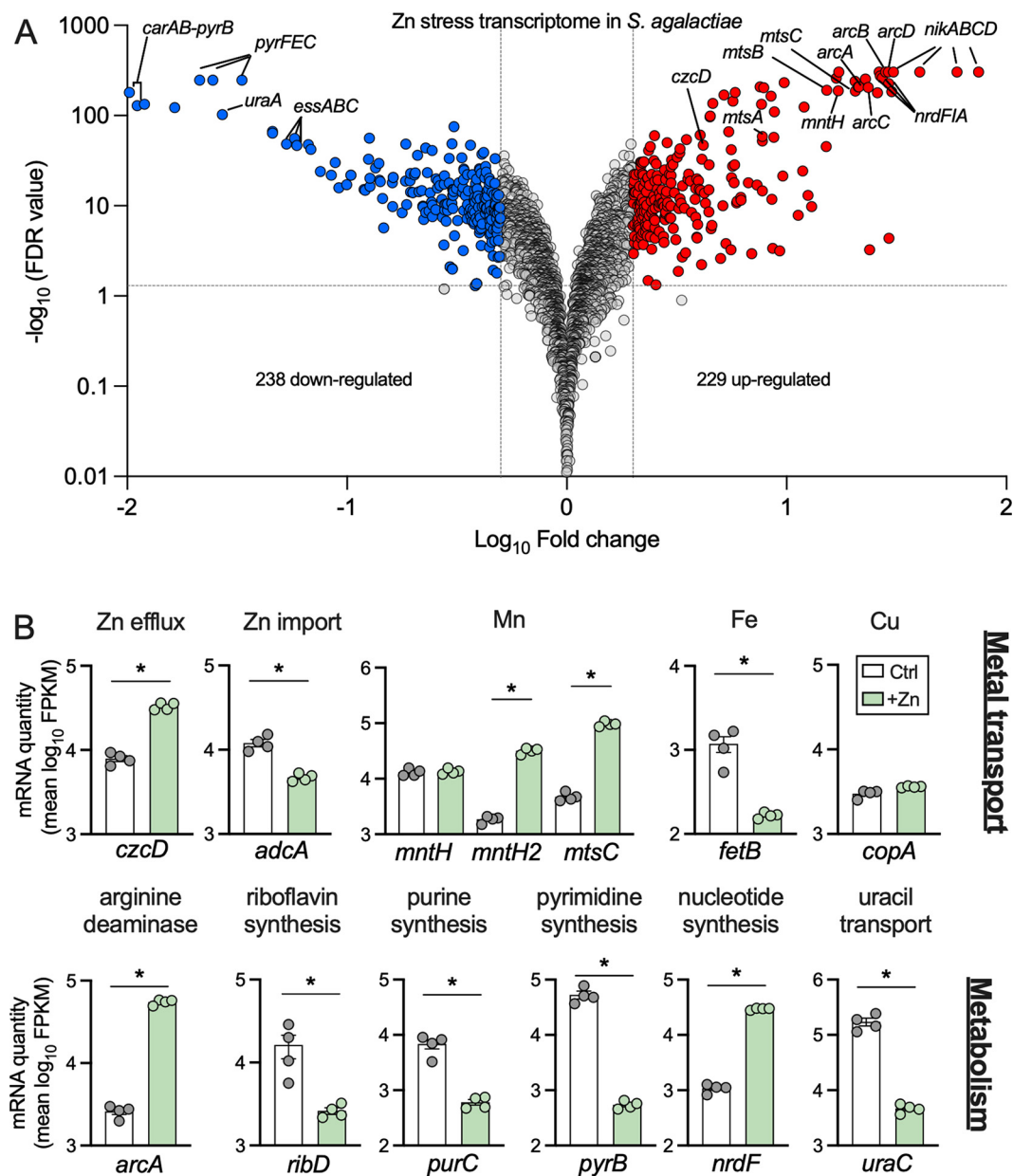


FIG 5 Transcriptomic analysis of *S. agalactiae* in Zn stress. (A) Volcano plot showing data from RNA-seq analysis of WT *S. agalactiae* cultures grown in medium containing 0.25 mM supplemental Zn compared to control cultures without supplemental Zn. Transcripts up- or downregulated in response to Zn ($n=4$; ± 2 -fold; $\text{FDR} < 0.05$) are highlighted in red and blue, respectively. Dotted lines show false discovery rate (FDR; q -value) and fold change cutoffs. Gray points indicate genes that were unchanged. Selected genes are identified individually with black lines. (B) Expression of selected genes from RNA-seq analyses showing mean fragments per kilobase of transcript per million mapped reads (FPKM) values for each condition, with predicted function as indicated. Data were compared with DESeq2 (*, $P\text{-adj} < 0.05$; ± 2 -fold).

hypothetical proteins of unknown function, some of which were up- or downregulated up to ~ 29 -fold. These observations represent a significant pool of targets for further studies in dissecting bacterial responses to Zn stress.

DISCUSSION

This study establishes a key role for cellular management of intracellular Zn levels in *S. agalactiae* via *czcD*, *sczA*, and additional mediators, including *arcA*, in conferring an ability to resist Zn intoxication to the bacteria. These findings provide new insight

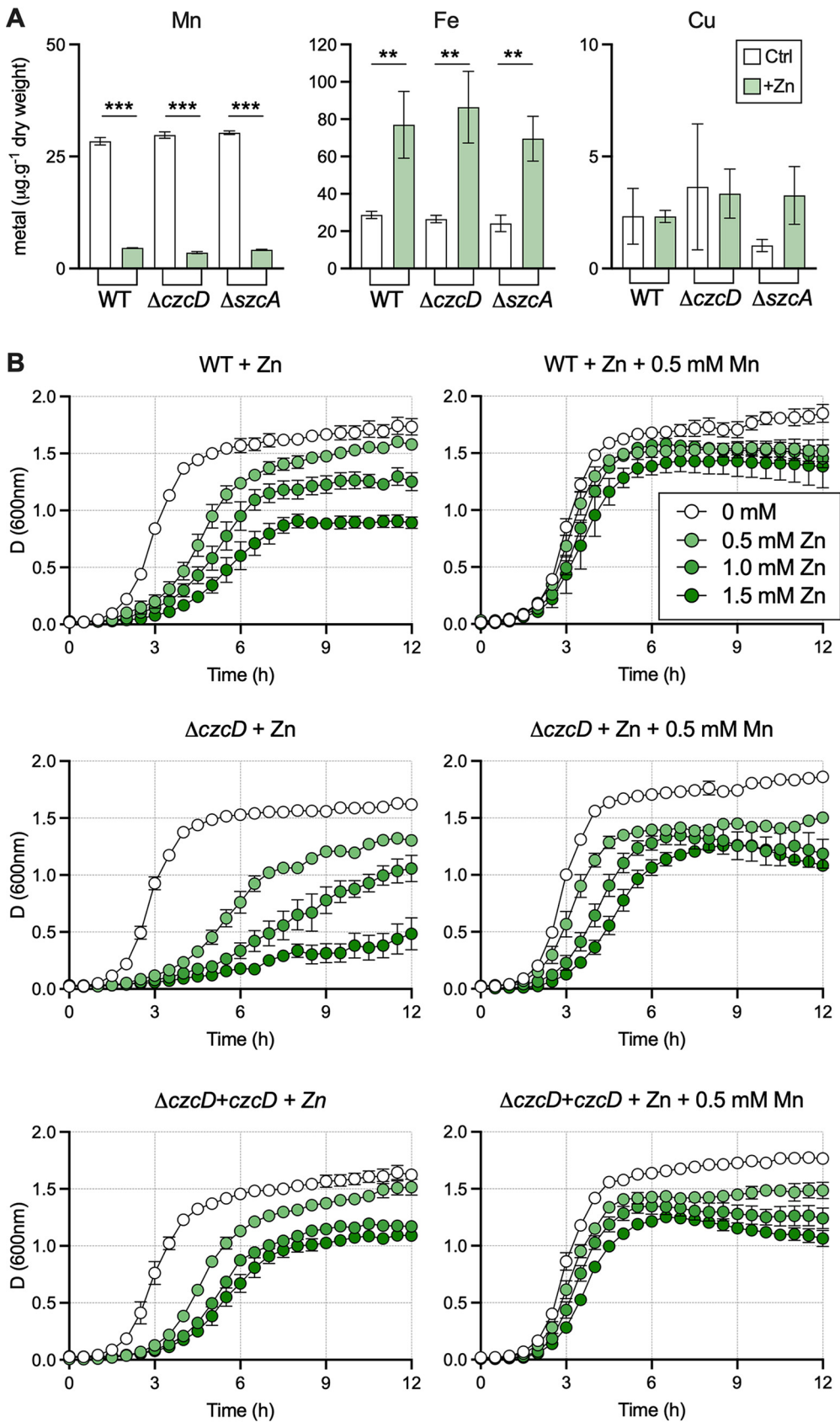


FIG 6 Intracellular metal accumulation during Zn stress and Mn rescue. (A) Intracellular accumulation of Mn, Fe, and Cu was compared with and without Zn supplementation in WT, $\Delta czcD$, and $\Delta szcA$ *S. agalactiae* strains using (Continued on next page)

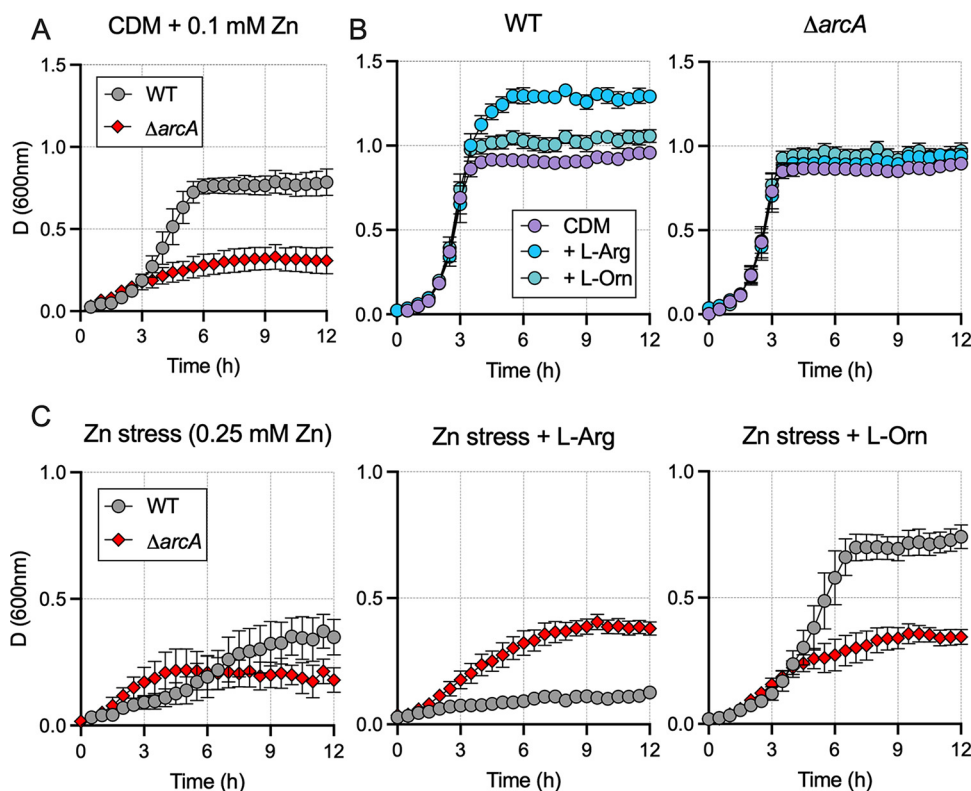


FIG 7 Comparisons of the growth of WT *S. agalactiae* and an $\Delta arcA$ isogenic mutant. (A) Cultures of WT and $\Delta arcA$ *S. agalactiae* were grown in nutrient-limited CDM under moderate Zn stress (± 0.1 mM Zn). (B) Cells were grown in CDM (without Zn) or CDM supplemented with 10 mM L-arginine or 10 mM L-ornithine. L-Arginine, but not L-ornithine, supplementation increases growth yield and final culture densities in the WT but not the $\Delta arcA$ strain. (C) WT and $\Delta arcA$ *S. agalactiae* were grown under conditions of severe Zn stress (+0.25 mM Zn) in CDM, with or without supplementation with 10 mM L-arginine or 10 mM L-ornithine. L-Ornithine rescues Zn sensitivity compared to 10 mM L-arginine or nonsupplemented controls. Data shown are mean measurements of attenuation (*D*; at 600 nm) from 3 to 4 independent experiments.

into the molecular mechanisms of virulence used by this pathogen to survive under stressful environmental conditions resulting from elevated metal ion levels, such as those within phagocytes during infection in a host. In characterizing the Zn efflux systems of *S. agalactiae* in detail, the findings of the present study support prior findings from work on other streptococci (17, 18); for example, our characterization of regulatory functions of *sczA* that enable cellular management of Zn in *S. agalactiae* are consistent with prior findings reported for *S. pyogenes* (17). These prior observations include that Zn stress upregulates Zn efflux via *czcD* and shuts down Zn uptake via *adcA* (24), with direct effects on the control of intracellular Zn content. Importantly, the Zn stress-response global transcriptome of *S. agalactiae* defined in the current study also elucidates other metal ion transporters and novel additional targets that have not previously been linked to Zn intoxication in any bacteria. A model of the Zn stress response in *S. agalactiae* based on the findings of this study is shown in Fig. 8.

Systems for Zn acquisition in *S. agalactiae* enable survival of the organism under Zn-deficient conditions (9) and confer resistance to calprotectin-mediated metal ion

FIG 6 Legend (Continued)

ICP-OES. Bars show means and SEM from 3 to 4 independent experiments and were compared by ordinary one-way ANOVA with Holm-Sidak multiple comparisons (**, $P < 0.01$; ***, $P < 0.001$). (B) Manganese supplementation rescues Zn toxicity in *S. agalactiae*. Growth comparisons of WT, $\Delta czcD$, and $\Delta czcD + czcD$ strains in THB or THB supplemented with 0.5, 1.0, or 1.5 mM Zn compared to the same medium but additionally supplemented with 0.5 mM Mn. Data are means and SEM from three independent experiments.

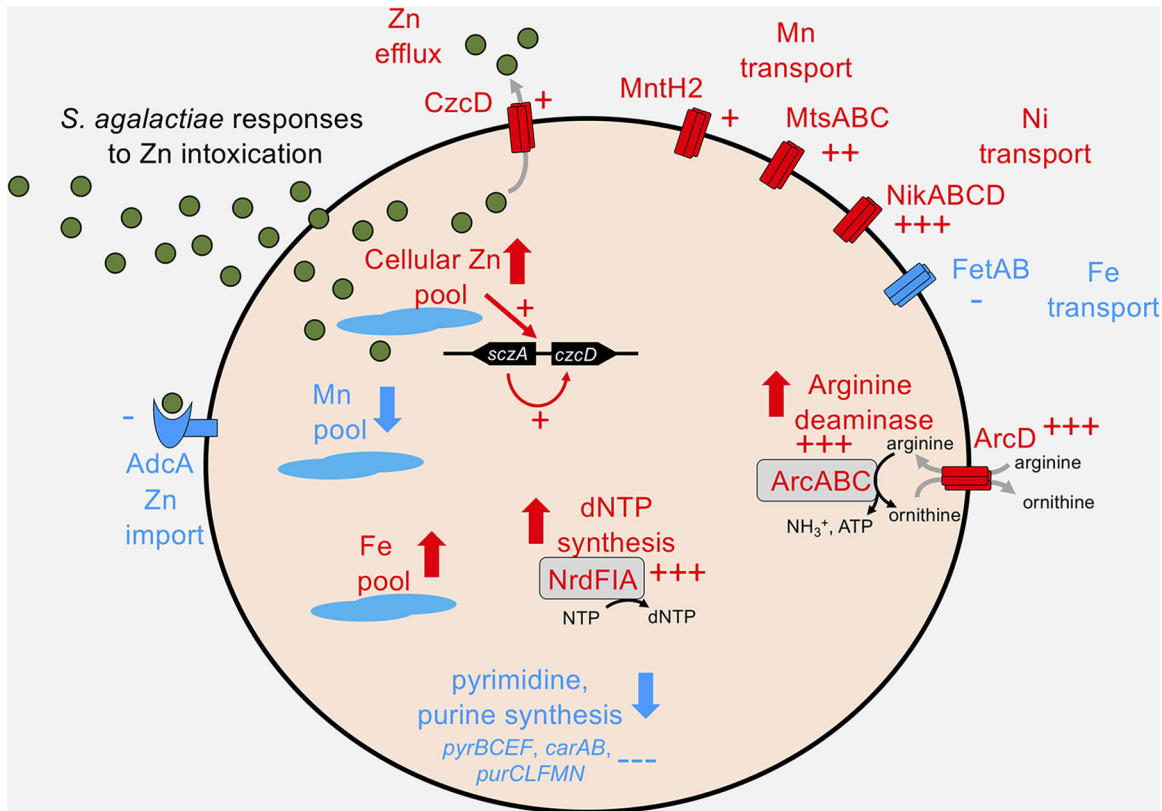


FIG 8 Summary of selected *S. agalactiae* responses to Zn intoxication. *S. agalactiae* senses elevated intracellular Zn to coordinate enhanced CzcD expression via the Zn-sensing SczA regulator. Zn stress results in a number of notable changes, including differential expression of metal transporters, altered Zn, Mn, and Fe cellular pools, and metabolic pathways encompassing arginine deaminase, *de novo* purine and pyrimidine syntheses, and dNTP synthesis. Red coloring and arrows indicate upregulation (+, 2- to 10-fold; ++, 10- to 20-fold; +++, >20-fold) or downregulation (-, 2 to 10-fold; -, >20-fold) of a transcript or process.

starvation (21), which acts to withhold multiple metals, such as Mn and Zn, from bacteria in the host (25). Our Zn intoxication transcriptional analyses identified numerous metal transporters that are differentially regulated, including *nikABCD* and *mtsABC*, predicted to transport Ni and Mn, respectively. Experiments in which we used supplemental Mn in the growth media revealed a rescue of the Zn sensitivity of the *czcD* mutant, further pointing to potentially important roles for such transporters. Given that Ni and Mn import genes have been implicated in bacterial survival during calprotectin stress (21), it is possible that *nik* and *mts* genes respond to altered cellular levels of other metals (rather than Zn) that occur as a consequence of Zn intoxication.

In our study, levels of cellular Mn were perturbed during Zn intoxication. This coincided with corresponding upregulation of *mntH2* and *mtsABC* transcription, encoding putative Mn transporters. Interestingly, some, but not all, *S. agalactiae* strains possess two genes encoding proteins homologous to NRAMP-type MntH transporters. *mntH* (CHF17_00875, [ASZ01148.1](#)) contributes to acid stress responses (26), but a role for *mntH2* (CHF17_02002, [ASZ02237.1](#)) has not been determined. In addition, *S. agalactiae* elevated Fe levels in response to Zn stress, coinciding with downregulation of a putative Fe export system encoded by *fetA-fetB*. In contrast, Cu levels and expression of *copA* (encoding a putative Cu transporter) were unaffected in *S. agalactiae* grown under Zn stress conditions. Collectively, these data show broader dysregulation of metal management in *S. agalactiae* undergoing Zn intoxication beyond Zn itself, encompassing Mn and Fe, consistent with a prior report on pneumococci (14). Future examination of the roles of the Ni, Mn, Fe, and Cu transport in *S. agalactiae* in the setting of bacterial metal stress and in models of infection would be of interest.

The finding that numerous core metabolic pathways in *S. agalactiae* are impacted by Zn stress, including some related to synthesis of purines, pyrimidines, riboflavin, and deoxynucleoside triphosphates, underscores the critical nature of Zn management for maintenance of basic cellular processes in the bacteria. The arginine deaminase system was among the most differentially regulated gene clusters, undergoing 20- to 30-fold enhanced expression during Zn stress. Remarkably, *arcA*-deficient *S. agalactiae* exhibited heightened sensitivity to Zn stress, establishing a novel role for this system in streptococcal resistance to metal ion intoxication. The precise molecular mechanisms that underpin how this system renders the bacterial cell resistant to Zn intoxication requires further definition, but arginine deaminase typically converts arginine to ammonia, ATP, and ornithine; overproduction of one of these may support bacterial survival during Zn stress. Consistent with this theory, we observed rescue of Zn sensitivity in *S. agalactiae* by supplementation with ornithine but not arginine. This interesting observation will require further examination in future work. A recent study identified arginine deaminase as a key factor in resistance to antibiotics and biofilm formation in *S. pyogenes* (27). Numerous prior studies have reported elevated expression of *arc* genes in *S. agalactiae* in response to acid stress (28), human serum (29), blood (30), or amniotic fluid (31). This suggests important but yet-to-be defined roles for arginine deaminase in the virulence of *S. agalactiae*. Together with the findings of the current study, these observations suggest that arginine deaminase supports the ability of *S. agalactiae* to respond to diverse stressors in addition to Zn intoxication.

Analysis of the role for Zn efflux systems of *S. agalactiae* in pathogenesis showed no contribution to bacterial survival in macrophages. This finding is surprising in the context of a prior study of *S. pneumoniae sczA* (that is functionally analogous to *S. agalactiae sczA*), which reported a major role for Zn cellular management via *sczA* in the intracellular survival of the bacteria in human macrophages (19). We confirmed the generation of a robust Zn mobilization response in the host cells following *S. agalactiae* infection but observed equivalent fitness of mutants for Zn management compared to the WT for survival in murine and human macrophages. Considering the conserved nature of *sczA* between streptococci, it is plausible that these mutants are attenuated in other phagocytes, such as neutrophils, as described for *S. pyogenes* (17), noting a need for further examination of differences in metal ion resistance phenotypes among streptococcal species.

The discovery of attenuation for colonization in a mouse model of disseminated infection in the *S. agalactiae* mutants in Zn management systems in this study suggests a role for Zn stress in disease pathogenesis due to this organism. The attenuations observed for the *czcD* and *sczA* mutants in the liver and bladder and the blood and heart, respectively, were not dramatic according to the tissue bacterial loads subsequent to blood challenge; however, the attenuations were statistically significant. Prior studies have shown more dramatic effects of *czcD* and *sczA* mutations in reducing bacterial virulence in mouse models of infection. For example, *czcD* mutation rendered *S. pyogenes* nonlethal in a subcutaneous infection model in mouse (17). *czcD* mutation attenuated *S. pneumoniae* 2.6-fold for survival in the lungs of mice following intranasal challenge compared to WT bacteria (32). Evaluating the current findings in the context of these prior studies highlights the differences in experimental designs, *viz.*, types of infection models, bacterial species, and outcome measures that would likely influence any potential degree of attenuation in mutants (17, 19, 32). For example, dietary zinc can influence bacterial colonization and/or survival, as shown in a murine model of infection with pneumococcus (32); in our study, we used a standard fixed-formulation diet (trace mineral content, in mg/kg of body weight: Mg, 100; Fe, 70; Cu, 16; I, 0.5; Mg, 70; Zn, 60; Mo, 0.5; Se, 0.1), and it possible that modifications to the trace mineral content of this diet will lead to different levels of recovery of bacteria in our model. We recognize this as a limitation of our study. More broadly, this highlights the importance of evaluating the roles of individual mediators, such as *CzcD*, *SczA*, and *ArcA*, in appropriate experimental models that are designed to parallel natural infection in the human

host. For *S. agalactiae*, for example, exploration of the role of resistance to Zn stress in colonization of the female genital tract (33) and the brain (34) would be of interest given the propensity of this pathogen to cause these infections in humans (35).

In conclusion, this study identifies new mediators of Zn cellular management in *S. agalactiae* and shows that resistance to Zn stress in this pathogen contributes to colonization in the host. Future examination of these mediators, and their role in the survival of *S. agalactiae* and other bacterial pathogens in relevant settings of infection, will be important to more fully understand microbial resistance to metal intoxication and its influence on virulence and pathogenesis.

MATERIALS AND METHODS

Bacterial strains, plasmids, and growth conditions. *S. agalactiae*, *Escherichia coli*, and plasmids used are listed in Table S1 in the supplemental material. *S. agalactiae* was routinely grown in Todd-Hewitt broth (THB) or on TH agar (1.5%, wt/vol). *E. coli* was grown in lysogeny broth (LB) or on LB agar. Media were supplemented with antibiotics (spectinomycin [Sp], 100 μ g/ml; chloramphenicol [Cm], 10 μ g/ml), as indicated. Growth assays used 200- μ l culture volumes in 96-well plates (Greiner) sealed using Breathe-Easy membranes (Sigma-Aldrich) and measured attenuation (*D*; at 600 nm) using a ClarioSTAR multimode plate reader (BMG Labtech). Attenuance measurements used well-scan mode with a 3-mm, 5-by-5 scan matrix, 5 flashes per point, path length correction of 5.88 mm, and 300-rpm agitation every 30 min. Media for growth assays were THB and a CDM (9), modified in the current study to include final concentrations of 1 g/liter glucose, 0.11 g/liter pyruvate, and 50 μ g/liter L-cysteine. For metal ion assays, the media were supplemented with Zn (supplied as ZnSO₄), Mn (supplied as MnCl₂), L-arginine, or L-ornithine as indicated. For attenuation baseline correction, control wells without bacteria were included for Zn in medium alone.

DNA extraction and genetic modification of *S. agalactiae*. Plasmid DNA was isolated using mini-prep kits (Qiagen), with modifications for *S. agalactiae* as described elsewhere (36). Electroporation of *S. agalactiae* and selection of transformants was performed as described previously (37). Deletion of *czcD* (CHF17_00567/CHF17_RS02855, [ASZ00854.1](#)) was performed by allelic exchange with a Cm cassette using pHY304aad9 as described previously (37). Briefly, ~400- to 500-bp regions upstream and downstream of *czcD* were amplified using primers (Table S2) carrying 21- to 23-bp overlapping sequence complementary to the Cm cassette of pLZ12 to facilitate fusion of these amplicons to chloramphenicol acetyltransferase by 3-way PCR. The subsequent product was cloned into pHY304aad9. Constructs for *sczA* and *arcA* deletions were made with DNA that was first synthesized in pUC57 by GenScript (USA), encompassing 500 bp of sequence upstream of either *sczA* or *arcA* fused to 500 bp of downstream sequence (Fig. S1) prior to subcloning into pHY304aad9. In-frame, markerless deletions in *sczA* and *arcA* were generated similarly by exploiting temperature selection using pHY304aad9, followed by loss of Sp resistance to identify double-crossover mutants. Constructs, complement plasmids, and primers are listed in Table S2. Mutants were validated by PCR using primers external to the mutation site and DNA sequencing.

Expression system for mCherry in *S. agalactiae*. Plasmid pGU2665 was designed for expressing mCherry in *trans* in *S. agalactiae* from the pCP25 promoter (38) cloned into pDL278 (39) (Fig. S2). Plasmid DNA was manipulated, and ligation reactions were performed essentially as described elsewhere (36). We verified pGU2665 by restriction analysis and sequencing using primers listed in Table S2. Sequence reads were mapped and assembled using Sequencher software. Plasmid stability assays were performed as described previously (36).

RNA extraction, qRT-PCR. For Zn exposure experiments, 1-ml overnight THB cultures were back-diluted 1/100 in 100 ml of THB (prewarmed at 37°C in 250-ml Erlenmeyer flasks) supplemented with 0.25, 0.5, 1.0, or 1.5 mM Zn. Cultures were grown with shaking (200 rpm) at 37°C; after exactly 2.5 h, 10- to 50-ml volumes containing approximately 500 million mid-log-phase bacteria were harvested; RNA was preserved and isolated as described previously (40). RNA quality was analyzed by RNA LabChip using GX Touch (Perkin Elmer). RNA (1,000 ng) was reverse transcribed using Superscript IV according to the manufacturer's instructions (Life Technologies), and cDNA was diluted 1:50 in water prior to quantitative PCR. Primers (Table S2) were designed using Primer3 Plus (41, 42) to quantify transcripts using Universal SYBR green supermix (Bio-Rad) and a Quantstudio 6 Flex (Applied Biosystems) system in accordance with MIQE guidelines (43). Standard curves were generated using five point serial dilutions of genomic DNA (5-fold) from WT *S. agalactiae* 874391 (44). Expression ratios were calculated using threshold cycle (*C_t*) values and primer efficiencies, as described elsewhere (45), using *dnaN*, encoding DNA polymerase III β -subunit as a housekeeper gene.

Whole bacterial cell metal content determination. Metal content in cells was determined as described previously (14), with minor modifications. Cultures were prepared essentially as described for RNA extraction and qRT-PCR, with the following modifications. THB medium was supplemented with 0.25 mM ZnSO₄ or not supplemented (Ctrl), and, following exposure for 2.5 h, bacteria were harvested by centrifugation at 4,122 $\times g$ at 4°C. Cell pellets were washed 3 times in phosphate-buffered saline (PBS) plus 5 mM EDTA to remove extracellular metals, followed by 3 washes in PBS. Pelleted cells were dried overnight at 80°C and resuspended in 1 ml of 32.5% nitric acid and incubated at 95°C for 1 h. The metal ion-containing supernatant was collected by centrifugation (14,000 $\times g$, 30 min) and diluted to a final concentration of 3.25% nitric acid for metal content determination using inductively coupled

plasma optical emission spectroscopy (ICP-OES). ICP-OES was carried out on an Agilent 720 ICP-OES with an axial torch, OneNeb concentric nebulizer, and Agilent single-pass glass cyclone spray chamber. The power was 1.4 kW with 0.75 liters/min nebulizer gas, 15 liters/min plasma gas, and 1.5 liters/min auxiliary gas flow. Zn was analyzed at 213.85 nm, Cu at 324.75 nm, Fe at 259.94 nm, and Mn at 257.61 nm, with detection limits at <1.1 ppm. The final quantity of each metal was normalized using dry weight biomass of the cell pellet prior to nitric acid digestion, expressed as micrograms per gram of dry weight. Baseline concentrations of Zn, Fe, Mn, and Cu in standard THB or CDM used in this study were determined from 3 independent assays (Table S3).

RNA sequencing and bioinformatics. Cultures were prepared as described above for RNA extraction and qRT-PCR. RNase-free DNase-treated RNA that passed Bioanalyzer 2100 (Agilent) analysis was used for RNA sequencing (RNA-seq) using the Illumina NextSeq 500 platform. We used TruSeq library generation kits (Illumina, San Diego, CA). Library construction consisted of random fragmentation of the poly(A) mRNA, followed by cDNA synthesis using random primers. The ends of the cDNA were repaired and A-tailed, and adaptors were ligated for indexing (with up to 12 different barcodes per lane) during the sequencing runs. The cDNA libraries were quantitated using quantitative PCR in a Roche LightCycler 480 with the Kapa Biosystems kit (Kapa Biosystems, Woburn, MA) prior to cluster generation. Clusters were generated to yield approximately 725K to 825K clusters/mm². Cluster density and quality were determined during the run after the first base addition parameters were assessed. We ran single-end 75-bp sequencing runs to align the cDNA sequences to the reference genome. For data preprocessing and bioinformatics, STAR (version 2.7.3a) was used (parameters used were `-outReadsUnmapped Fastx -outSAMtype BAM SortedByCoordinate -outSAMattributes All`) to align the raw RNA sequencing fastq reads to the WT *S. agalactiae* 874391 reference genome (44). HTSeq-count, version 0.11.1 (parameters used were `-r pos -t exon -i gene_id -a 10 -s no -f bam`), was used to estimate transcript abundances (46). DESeq2 was then used to normalize and test for differential expression and regulation following their vignette. Genes that met certain criteria (i.e., fold change of more than ± 2.0 , q value of <0.05) were accepted as significantly altered (47).

Mammalian cell culture. J774A.1 murine macrophages or U937 human monocyte-derived macrophages (MDMs) were grown in RPMI and seeded (10^5) into the wells of a 96-well tissue culture-treated plate (Falcon) essentially as described elsewhere (48, 49), except that U937 MDMs were differentiated by exposure to 50 ng/ml phorbol 12-myristate 13-acetate (PMA) for 48 h and cells subsequently rested in media without PMA for 72 h to enhance morphological and phenotypic markers of MDMs (50). A multiplicity of infection (MOI) of 100 bacteria to macrophage for 1 h was used in RPMI without antibiotics. Nonadherent bacteria were removed by five washes of 200 μ l PBS using a Well Wash Versa (Thermo Scientific). RPMI containing 250 U/ml penicillin, streptomycin (Gibco), and 50 μ g/ml gentamicin (Sigma-Aldrich) was used for antibiotic protection assays to quantify intracellular bacteria as described previously (49). At 1 h, 24 h, or 48 h after infection, monolayers were washed five times with 200 μ l PBS and lysed by brief exposure to 50 μ l of 2% trypsin and 0.02% Triton X-100 (10 min) prior to dilution with 150 μ l PBS and estimation of the number of CFU per milliliter by serial dilution and plate counts on agar.

Fluorescence microscopy. Fifty thousand J774A.1 cells were seeded into 8-well LabTek II chamber slides (Nunc) and infected with mCherry-*S. agalactiae* for 1 h, followed by washing and application of antibiotics according to the antibiotic protection assay as described above. Then, 24 h later, the infected cells were subjected to three washes of 200 μ l PBS and fixed for 15 min at 37°C using 4% (wt/vol) paraformaldehyde. Monolayers were stained for Zn²⁺ using 5 μ M FluoZin-3 AM (Life Technologies) for 30 min at 37°C and subsequently for DNA using Hoechst 33258 for 5 min. Fixed, stained cells were washed twice in PBS and mounted using *n*-propyl gallate (*n*-pg) mounting medium (0.2% *n*-pg in 9:1 glycerol-PBS). mCherry-*S. agalactiae* was visualized using a Zeiss AxioImager.M2 microscope (Carl Zeiss MicroImaging) fitted with Plan-Apochromat X20/0.8 and X63/1.40 lens objectives and an AxioCam MRm Rev.3 camera. Images of cells were captured with 63HE, 44, and 49 filter sets (to detect mCherry [587 nm, 610 nm], FluoZin-3 [494 nm, 518 nm], and Hoechst 33258 [352 nm, 461 nm] fluorescence, respectively, with excitation and emission spectra listed consecutively for each) and Zen Pro (version 2) software.

Animals and ethics statement. Virulence was tested using a mouse model of disseminated infection based on intravenous challenge as described elsewhere (20). Briefly, an inoculum of 10^7 *S. agalactiae* in 200 μ l of PBS (pH 7.4) was delivered to each mouse via the lateral tail vein using a 1-ml syringe connected to a 27-gauge by 1.25-inch regular wall needle. This study was carried out in accordance with the guidelines of the Australian National Health and Medical Research Council. The Griffith University Animal Ethics Committee reviewed and approved all experimental protocols for animal usage according to the guidelines of the National Health and Medical Research Council (approval MSC/01/18/AEC).

Statistical methods. All statistical analyses used GraphPad Prism V8 and are defined in the respective figure legends. Statistical significance was accepted at P values of ≤ 0.05 .

Data availability. Raw and processed data were deposited in the Gene Expression Omnibus (accession no. [GSE161127](https://www.ncbi.nlm.nih.gov/geo/query/acc.cgi?acc=GSE161127) for wild-type [WT] *S. agalactiae* 874391 during Zn intoxication; [GSE167894](https://www.ncbi.nlm.nih.gov/geo/query/acc.cgi?acc=GSE167894) for WT *S. agalactiae* 874391 control).

SUPPLEMENTAL MATERIAL

Supplemental material is available online only.

FIG S1, TIF file, 0.9 MB.

FIG S2, TIF file, 0.7 MB.

FIG S3, TIF file, 0.3 MB.

FIG S4, TIF file, 0.2 MB.

TABLE S1, DOCX file, 0.02 MB.

TABLE S2, DOCX file, 0.01 MB.

TABLE S3, DOCX file, 0.01 MB.

TABLE S4, XLSX file, 0.05 MB.

ACKNOWLEDGMENTS

We thank Michael Crowley, David Crossman, and Koo Hyunmin of the Hefflin Centre for Genomic Science Core Laboratories, University of Alabama at Birmingham (Birmingham, AL), for RNA sequencing. We thank Timothy Barnett for providing pLZ12 containing cloned mCherry. We also thank Lahiru Katupitiya and Dean Gosling for excellent technical assistance and Ryan Stewart at the School of Environment and Science, Griffith University, for ICP-OES.

This work was supported by a Project Grant from the National Health and Medical Research Council (NHMRC) Australia (APP1146820 to G.C.U.).

REFERENCES

1. Watly J, Potocki S, Rowinska-Zyrek M. 2016. Zinc homeostasis at the bacteria/host interface—from coordination chemistry to nutritional immunity. *Chemistry* 22:15992–16010. <https://doi.org/10.1002/chem.201602376>.
2. Osman D, Cavet JS. 2008. Copper homeostasis in bacteria. *Adv Appl Microbiol* 65:217–247. [https://doi.org/10.1016/S0065-2164\(08\)00608-4](https://doi.org/10.1016/S0065-2164(08)00608-4).
3. Chandransu P, Rensing C, Helmann JD. 2017. Metal homeostasis and resistance in bacteria. *Nat Rev Microbiol* 15:338–350. <https://doi.org/10.1038/nrmicro.2017.15>.
4. German N, Doyscher D, Rensing C. 2013. Bacterial killing in macrophages and amoeba: do they all use a brass dagger? *Future Microbiol* 8:1257–1264. <https://doi.org/10.2217/fmb.13.100>.
5. Djoko KY, Ong CL, Walker MJ, McEwan AG. 2015. The role of copper and zinc toxicity in innate immune defense against bacterial pathogens. *J Biol Chem* 290:18954–18961. <https://doi.org/10.1074/jbc.R115.647099>.
6. Ladomersky E, Petris MJ. 2015. Copper tolerance and virulence in bacteria. *Metallomics* 7:957–964. <https://doi.org/10.1039/c4mt00327f>.
7. Besold AN, Culbertson EM, Culotta VC. 2016. The Yin and Yang of copper during infection. *J Biol Inorg Chem* 21:137–144. <https://doi.org/10.1007/s00775-016-1335-1>.
8. Bayle L, Chimalapati S, Schoehn G, Brown J, Vernet T, Durmort C. 2011. Zinc uptake by *Streptococcus pneumoniae* depends on both AdcA and AdcAll and is essential for normal bacterial morphology and virulence. *Mol Microbiol* 82:904–916. <https://doi.org/10.1111/j.1365-2958.2011.07862.x>.
9. Moulin P, Patron K, Cano C, Zorgani MA, Camiade E, Borezee-Durant E, Rosenau A, Meregheggi L, Hiron A. 2016. The Adc/Lmb system mediates zinc acquisition in *Streptococcus agalactiae* and contributes to bacterial growth and survival. *J Bacteriol* 198:3265–3277. <https://doi.org/10.1128/JB.00614-16>.
10. Zygiel EM, Nolan EM. 2018. Transition metal sequestration by the host-defense protein calprotectin. *Annu Rev Biochem* 87:621–643. <https://doi.org/10.1146/annurev-biochem-062917-012312>.
11. Kapetanovic R, Bokil NJ, Achard ME, Ong CL, Peters KM, Stocks CJ, Phan MD, Monteleone M, Schroder K, Irvine KM, Saunders BM, Walker MJ, Stacey KJ, McEwan AG, Schembri MA, Sweet MJ. 2016. *Salmonella* employs multiple mechanisms to subvert the TLR-inducible zinc-mediated antimicrobial response of human macrophages. *FASEB J* 30:1901–1912. <https://doi.org/10.1096/fj.201500061>.
12. Achard Maud ES, Stafford Sian L, Bokil Nilesh J, Chartres J, Bernhardt Paul V, Schembri Mark A, Sweet Matthew J, McEwan Alastair G. 2012. Copper redistribution in murine macrophages in response to *Salmonella* infection. *Biochem J* 444:51–57. <https://doi.org/10.1042/BJ20112180>.
13. McDevitt CA, Ogunniyi AD, Valkov E, Lawrence MC, Kobe B, McEwan AG, Paton JC. 2011. A molecular mechanism for bacterial susceptibility to zinc. *PLoS Pathog* 7:e1002357. <https://doi.org/10.1371/journal.ppat.1002357>.
14. Eijkelkamp BA, Morey JR, Ween MP, Ong CL, McEwan AG, Paton JC, McDevitt CA. 2014. Extracellular zinc competitively inhibits manganese uptake and compromises oxidative stress management in *Streptococcus pneumoniae*. *PLoS One* 9:e89427. <https://doi.org/10.1371/journal.pone.0089427>.
15. Ong CL, Walker MJ, McEwan AG. 2015. Zinc disrupts central carbon metabolism and capsule biosynthesis in *Streptococcus pyogenes*. *Sci Rep* 5:10799. <https://doi.org/10.1038/srep10799>.
16. Hassan KA, Pederick VG, Elbourne LD, Paulsen IT, Paton JC, McDevitt CA, Eijkelkamp BA. 2017. Zinc stress induces copper depletion in *Acinetobacter baumannii*. *BMC Microbiol* 17:59. <https://doi.org/10.1186/s12866-017-0965-y>.
17. Ong CL, Gillen CM, Barnett TC, Walker MJ, McEwan AG. 2014. An antimicrobial role for zinc in innate immune defense against group A streptococcus. *J Infect Dis* 209:1500–1508. <https://doi.org/10.1093/infdis/jiu053>.
18. Kloosterman TG, van der Kooi-Pol MM, Bijlsma JJ, Kuipers OP. 2007. The novel transcriptional regulator SczA mediates protection against Zn²⁺ stress by activation of the Zn²⁺-resistance gene czcD in *Streptococcus pneumoniae*. *Mol Microbiol* 65:1049–1063. <https://doi.org/10.1111/j.1365-2958.2007.05849.x>.
19. Martin JE, Edmonds KA, Bruce KE, Campanello GC, Eijkelkamp BA, Brazel EB, McDevitt CA, Winkler ME, Giedroc DP. 2017. The zinc efflux activator SczA protects *Streptococcus pneumoniae* serotype 2 D39 from intracellular zinc toxicity. *Mol Microbiol* 104:636–651. <https://doi.org/10.1111/mmi.13654>.
20. Sullivan MJ, Ulett GC. 2020. Evaluation of hematogenous spread and ascending infection in the pathogenesis of acute pyelonephritis due to group B streptococcus in mice. *Microb Pathog* 138:103796. <https://doi.org/10.1016/j.micpath.2019.103796>.
21. Burham LR, Le Breton Y, Radin JN, Spencer BL, Deng L, Hiron A, Ransom MR, Mendonca JDC, Belew AT, El-Sayed NM, McIver KS, KehI-Fie TE, Doran KS. 2020. Identification of zinc-dependent mechanisms used by group B *Streptococcus* to overcome calprotectin-mediated stress. *mBio* 11:e02302-20. <https://doi.org/10.1128/mBio.02302-20>.
22. Schulz C, Gierok P, Petruschka L, Lalk M, Mader U, Hammerschmidt S. 2014. Regulation of the arginine deiminase system by ArgR2 interferes with arginine metabolism and fitness of *Streptococcus pneumoniae*. *mBio* 5:e01858-14. <https://doi.org/10.1128/mBio.01858-14>.
23. Shabayek S, Spellerberg B. 2017. Acid stress response mechanisms of group B streptococci. *Front Cell Infect Microbiol* 7:395. <https://doi.org/10.3389/fcimb.2017.00395>.
24. Ong CY, Berking O, Walker MJ, McEwan AG. 2018. New insights into the role of zinc acquisition and zinc tolerance in group A streptococcal infection. *Infect Immun* 86:e00048-18. <https://doi.org/10.1128/IAI.00048-18>.
25. Corbin BD, Seeley EH, Raab A, Feldmann J, Miller MR, Torres VJ, Anderson KL, Dattilo BM, Dunman PM, Gerads R, Caprioli RM, Nacken W, Chazin WJ, Skaar EP. 2008. Metal chelation and inhibition of bacterial growth in tissue abscesses. *Science* 319:962–965. <https://doi.org/10.1126/science.1152449>.
26. Shabayek S, Bauer R, Mauerer S, MizaiKoff B, Spellerberg B. 2016. A streptococcal NRAMP homologue is crucial for the survival of *Streptococcus agalactiae* under low pH conditions. *Mol Microbiol* 100:589–606. <https://doi.org/10.1111/mmi.13335>.
27. Freiberg JA, Le Breton Y, Harro JM, Allison DL, McIver KS, Shirliff ME. 2020. The Arginine deiminase pathway impacts antibiotic tolerance

- during biofilm-mediated *Streptococcus pyogenes* infections. *mBio* 11: e00919-20. <https://doi.org/10.1128/mBio.00919-20>.
28. Santi I, Grifantini R, Jiang SM, Brettoni C, Grandi G, Wessels MR, Soriani M. 2009. CsrRS regulates group B *Streptococcus* virulence gene expression in response to environmental pH: a new perspective on vaccine development. *J Bacteriol* 191:5387–5397. <https://doi.org/10.1128/JB.00370-09>.
 29. Yang Q, Zhang M, Harrington DJ, Black GW, Sutcliffe IC. 2011. A proteomic investigation of *Streptococcus agalactiae* reveals that human serum induces the C protein beta antigen and arginine deiminase. *Microbes Infect* 13:757–760. <https://doi.org/10.1016/j.micinf.2011.03.001>.
 30. Mereghetti L, Sitkiewicz I, Green NM, Musser JM. 2008. Extensive adaptive changes occur in the transcriptome of *Streptococcus agalactiae* (group B streptococcus) in response to incubation with human blood. *PLoS One* 3: e3143. <https://doi.org/10.1371/journal.pone.0003143>.
 31. Sitkiewicz I, Musser JM. 2009. Analysis of growth-phase regulated genes in *Streptococcus agalactiae* by global transcript profiling. *BMC Microbiol* 9:32. <https://doi.org/10.1186/1471-2180-9-32>.
 32. Eijkelkamp BA, Morey JR, Neville SL, Tan A, Pederick VG, Cole N, Singh PP, Ong CY, Gonzalez de Vega R, Clases D, Cunningham BA, Hughes CE, Comerford I, Brazel EB, Whittall JJ, Plumpre CD, McColl SR, Paton JC, McEwan AG, Doble PA, McDavitt CA. 2019. Dietary zinc and the control of *Streptococcus pneumoniae* infection. *PLoS Pathog* 15:e1007957. <https://doi.org/10.1371/journal.ppat.1007957>.
 33. Carey AJ, Tan CK, Mirza S, Irving-Rodgers H, Webb RI, Lam A, Ulett GC. 2014. Infection and cellular defense dynamics in a novel 17beta-estradiol murine model of chronic human group B streptococcus genital tract colonization reveal a role for hemolysin in persistence and neutrophil accumulation. *J Immunol* 192:1718–1731. <https://doi.org/10.4049/jimmunol.1202811>.
 34. Lembo A, Gurney MA, Burnside K, Banerjee A, de los Reyes M, Connelly JE, Lin WJ, Jewell KA, Vo A, Renken CW, Doran KS, Rajagopal L. 2010. Regulation of CovR expression in group B *Streptococcus* impacts blood-brain barrier penetration. *Mol Microbiol* 77:431–443. <https://doi.org/10.1111/j.1365-2958.2010.07215.x>.
 35. Edwards MS, Baker CJ. 2018. *Streptococcus agalactiae* (group B *Streptococcus*), p 723–729. In Long SS, Prober CG, Fischer M (ed), *Principles and practice of pediatric infectious diseases* (5th ed). Elsevier, New York, NY. <https://doi.org/10.1016/B978-0-323-40181-4.00119-5>.
 36. Sullivan MJ, Ulett GC. 2018. Stable expression of modified green fluorescent protein in group B streptococci to enable visualization in experimental systems. *Appl Environ Microbiol* 84:e01262-18. <https://doi.org/10.1128/AEM.01262-18>.
 37. Ipe DS, Ben Zakour NL, Sullivan MJ, Beatson SA, Ulett KB, Benjamin WHJ, Davies MR, Dando SJ, King NP, Cripps AW, Schembri MA, Dougan G, Ulett GC. 2015. Discovery and characterization of human-urine utilization by asymptomatic-bacteriuria-causing *Streptococcus agalactiae*. *Infect Immun* 84:307–319. <https://doi.org/10.1128/IAI.00938-15>.
 38. Jensen PR, Hammer K. 1998. The sequence of spacers between the consensus sequences modulates the strength of prokaryotic promoters. *Appl Environ Microbiol* 64:82–87. <https://doi.org/10.1128/AEM.64.1.82-87.1998>.
 39. LeBlanc DJ, Lee LN, Abu-Al-Jaibat A. 1992. Molecular, genetic, and functional analysis of the basic replicon of pVA380-1, a plasmid of oral streptococcal origin. *Plasmid* 28:130–145. [https://doi.org/10.1016/0147-619x\(92\)90044-b](https://doi.org/10.1016/0147-619x(92)90044-b).
 40. Sullivan MJ, Leclercq SY, Ipe DS, Carey AJ, Smith JP, Voller N, Cripps AW, Ulett GC. 2017. Effect of the *Streptococcus agalactiae* virulence regulator CovR on the pathogenesis of urinary tract infection. *J Infect Dis* 215:475–483. <https://doi.org/10.1093/infdis/jiw589>.
 41. Untergasser A, Cutcutache I, Koressaar T, Ye J, Faircloth BC, Remm M, Rozen SG. 2012. Primer3—new capabilities and interfaces. *Nucleic Acids Res* 40:e115. <https://doi.org/10.1093/nar/gks596>.
 42. Untergasser A, Nijveen H, Rao X, Bisseling T, Geurts R, Leunissen JA. 2007. Primer3Plus, an enhanced web interface to Primer3. *Nucleic Acids Res* 35: W71–W74. <https://doi.org/10.1093/nar/gkm306>.
 43. Bustin SA, Benes V, Garson JA, Hellemans J, Huggett J, Kubista M, Mueller R, Nolan T, Pfaffl MW, Shipley GL, Vandesompele J, Wittwer CT. 2009. The MIQE guidelines: minimum information for publication of quantitative real-time PCR experiments. *Clin Chem* 55:611–622. <https://doi.org/10.1373/clinchem.2008.112797>.
 44. Sullivan MJ, Forde BM, Prince DW, Ipe DS, Ben Zakour NL, Davies MR, Dougan G, Beatson SA, Ulett GC. 2017. Complete genome sequence of serotype III *Streptococcus agalactiae* sequence type 17 strain 874391. *Genome Announc* 5:e01107-17. <https://doi.org/10.1128/genomeA.01107-17>.
 45. Pfaffl MW. 2001. A new mathematical model for relative quantification in real-time RT-PCR. *Nucleic Acids Res* 29:e45. <https://doi.org/10.1093/nar/29.9.e45>.
 46. Anders S, Pyl PT, Huber W. 2015. HTSeq—a Python framework to work with high-throughput sequencing data. *Bioinformatics* 31:166–169. <https://doi.org/10.1093/bioinformatics/btu638>.
 47. Love MI, Huber W, Anders S. 2014. Moderated estimation of fold change and dispersion for RNA-seq data with DESeq2. *Genome Biol* 15:550. <https://doi.org/10.1186/s13059-014-0550-8>.
 48. Acharya D, Sullivan MJ, Duell BL, Goh KKG, Katupitiya L, Gosling D, Chamoun MN, Kakkanat A, Chattopadhyay D, Crowley M, Crossman DK, Schembri MA, Ulett GC. 2019. Rapid bladder interleukin-10 synthesis in response to uropathogenic *Escherichia coli* is part of a defense strategy triggered by the major bacterial flagellar filament FlhC and contingent on TLR5. *mSphere* 4:e00545-19. <https://doi.org/10.1128/mSphere.00545-19>.
 49. Leclercq SY, Sullivan MJ, Ipe DS, Smith JP, Cripps AW, Ulett GC. 2016. Pathogenesis of *Streptococcus* urinary tract infection depends on bacterial strain and beta-hemolysin/cytolysin that mediates cytotoxicity, cytokine synthesis, inflammation and virulence. *Sci Rep* 6:29000. <https://doi.org/10.1038/srep29000>.
 50. Valdes Lopez JF, Urcuqui-Inchima S. 2018. Synergism between phorbol-12-myristate-13-acetate and vitamin D3 in the differentiation of U937 cells to monocytes and macrophages. *Morphologie* 102:205–218. <https://doi.org/10.1016/j.morpho.2018.06.001>.